Tapered fibertrodes: opto-electrical neural interfaces in small brain volumes with reduced artefacts

Barbara Spagnolo[1‡*], Antonio Balena [1‡], Rui T. Peixoto[3,4‡], Marco Pisanello[1‡], Leonardo Sileo[1], Marco Bianco[1,2], Alessandro Rizzo[1,2], Filippo Pisano[1], Antonio Qualtieri[1], Dario Domenico Lofrumento[5], Francesco De Nuccio[5], John A. Assad[3], Bernardo L. Sabatini[3], Massimo De Vittorio[1,2,†] and Ferruccio Pisanello[1,†]

1 – Istituto Italiano di Tecnologia, CBN, Arnesano, 73010 Lecce (Italy)

2 – Dipartimento di Ingegneria dell'Innovazione, Università del Salento, Lecce (Italy)

3- Howard Hughes Medical Institute, Department of Neurobiology, Harvard Medical School, Boston, MA 02115, (USA)

4- Department of Psychiatry, University of Pittsburgh, 450 Technology Dr, Pittsburgh, PA 15219, (USA)

5- DiSTeBA - Dept. of Biological and Environmental Sciences and Technologies. Università del Salento, Lecce (Italy)

[*] *Corresponding author, e-mail: barbara.spagnolo@iit.it, ferruccio.pisanello@iit.it, massimo.devittorio@iit.it*

[‡] *These authors equally contributed*

[†]*co-last author*

Supplementary Material

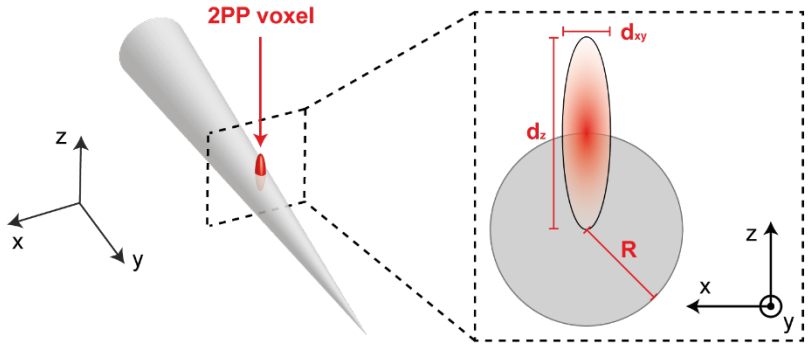

Supplementary Figure 1: 3D Sketch of a taper intersecting with a 2PP voxel. Inset: the 2D section of the taper at a radius of curvature R, intersecting with a voxel modeled as an ellipsis with lateral dimension d_{xy} and axial dimension d_z.

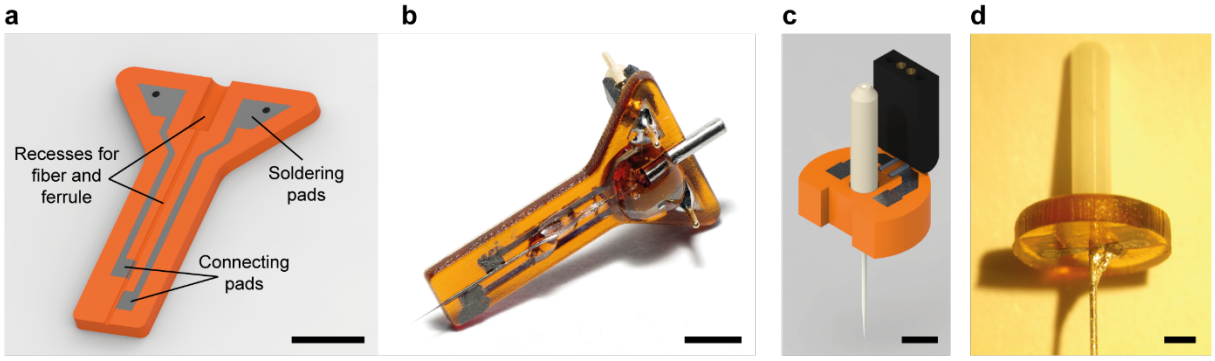

Supplementary Figure 2: Printed Circuit Board. (a) Rendering of a 3D printed PCB for acute implant; connection pads, soldering pads, and waveguide recesses are pointed out. Scalebar 5 mm. **(b)** Realized device with DIL pin connectors to interface with an electrophysiology headstage. Scalebar 5 mm. **(c)** Rendering and **(d)** device realized of a 3D printed PCB for chronically implantable devices with standard Omnetics connector for DAQ systems interfacing. Scalebars 2 and 1 mm.

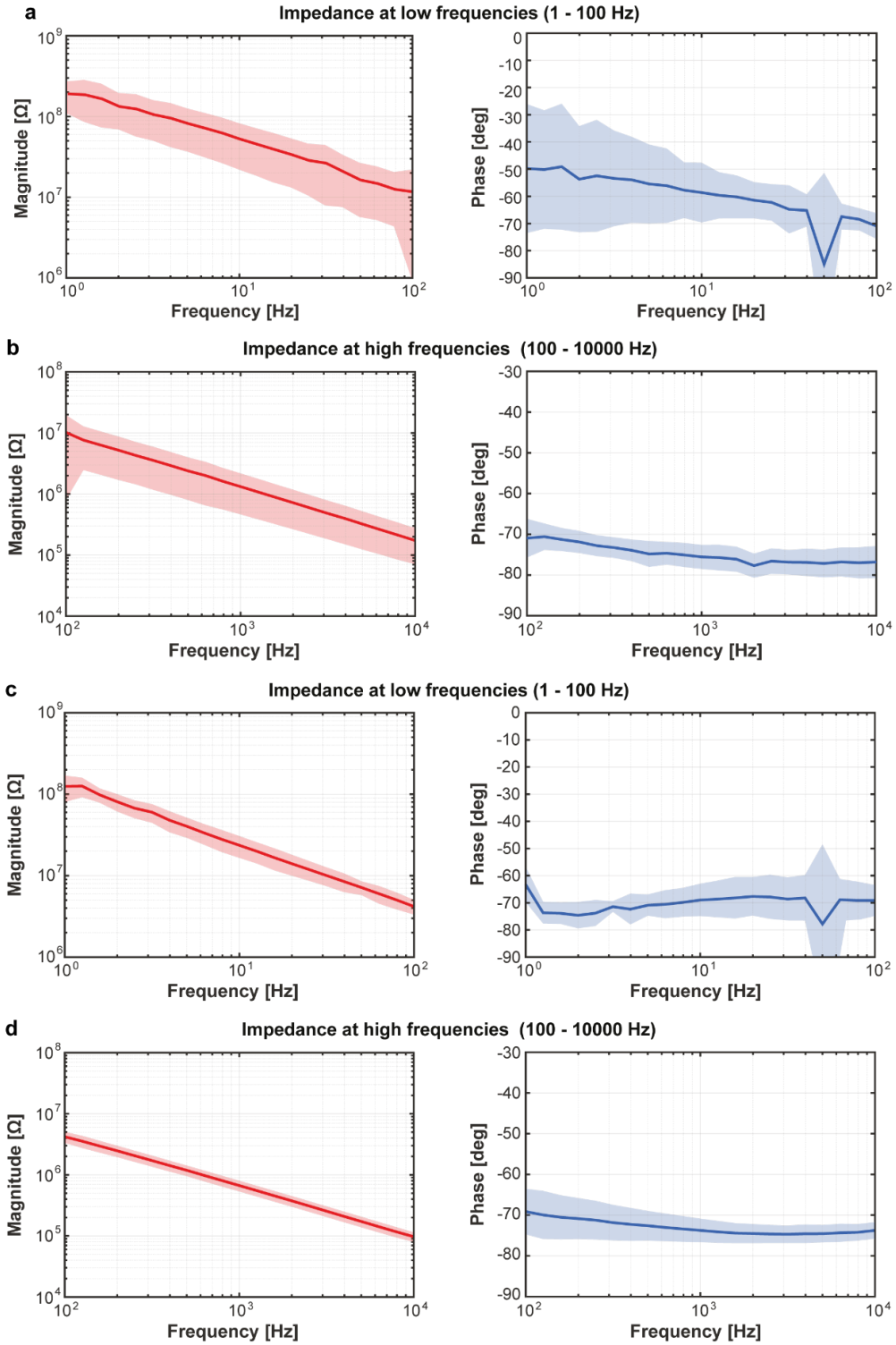

Supplementary Figure 3: 2PP Electrodes Impedance characterization. Statistical evaluation of average and standard deviation of **(left)** magnitude and **(right)** phase of electrochemical impedance spectroscopy measurements on n = 7 fibertrodes featuring a 15 µm-diameter recording site realized by 2PP **(a-b)** and by FIB **(c-d)**. In **(a)** and **(c)** the low frequency regime (1 – 100 Hz) is shown, while in **(b)** and **(d)** data for the frequency interval 100 - 10^4 Hz are reported.

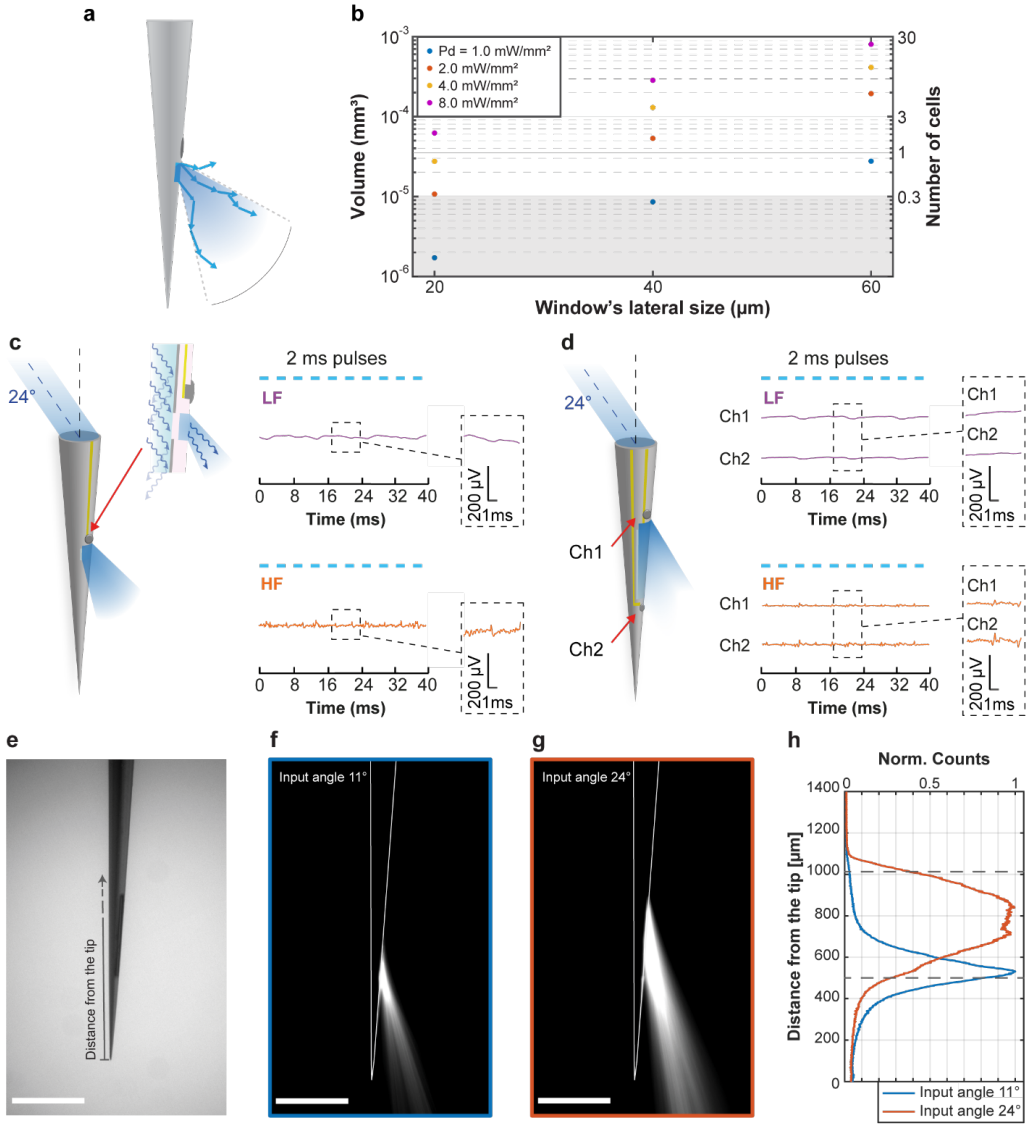

Supplementary Figure 4. (a,b) Numerical estimation of excitation volumes. (a) Schematic representation of photons propagation at the window exit: electrode area is located in the region of lowest power density and is not interested by backscattered light. 1000 photons packets, each made of 10^5 photons, were generated from a uniform distribution in the angular ranges $\theta_{OUT\ min,xz} < \theta_{OUT,xz} < \theta_{OUT\ max,xz}$ and $-\Delta\theta_{OUT,xy}/2 < \theta_{OUT,xy} < \Delta\theta_{OUT,xy}/2$ in the (x,z) and (x,y) planes. For the three window's size simulations were run with $\theta_{OUT\ min,xz} = 25°$, 21° and 27°, $\theta_{OUT\ max,xz} = 42°$, 38° and 33° and $\Delta\theta_{OUT,xy} = 18°$, 24° and 30° for 20 × 20 µm², 40 × 40 µm² and 60 × 60 µm² lateral size windows, respectively; the slot simulation was run with $\theta_{OUT\ min,xz} = 8°$, $\theta_{OUT\ max,xz} = 24°$, and $\Delta\theta_{OUT,xy} = 18°$. Brain tissue was modeled with a Henyey-Greenstein scattering function, with parameters n = 1.360, l = 90.16 µm, g = 0.89, T = 0.9874. **(b)** Estimation of volume enclosed by the iso-surface at 1 mW/mm² for different emitted average power densities and different window lateral sizes. Number of neurons related to the volumes are determined assuming a density of $3 \cdot 10^4$ neurons/mm³. **(c-d) Light induced photoelectric noise** in fibertrodes realized with 2PP, featuring **(c)** one window and one electrode and **(d)** two electrodes and a rectangular slot-like aperture. Delivery of short light pulses (2 ms) resulted in no artefacts detected in both the low

frequency (purple) and high frequency (orange) channels. **(e-h) Fibertrode with slot-like emission aperture fabricated through 2PP.** Brightfield image of the 500 µm-long slot-like window. The elongated shape of the aperture allows for redistributing outcoupled light depending on the injection angle **(f and g)** resulting in different emission profiles. The emitting length ($1/e^2$ of the relative maximum) for **(f)** is 203 µm with an input angle of 11°, and for **(g)** is 462 µm with an input angle of 24°. Scale bars in **a-c** are 500 µm. **(h)** Comparison of the normalized emission profile versus the distance from the fiber tip for the two input angles in **(f)** and **(g)**. Dashed lines indicate the extension of the slot aperture. Experiments in panels e-h were repeated n=3 times with similar results.

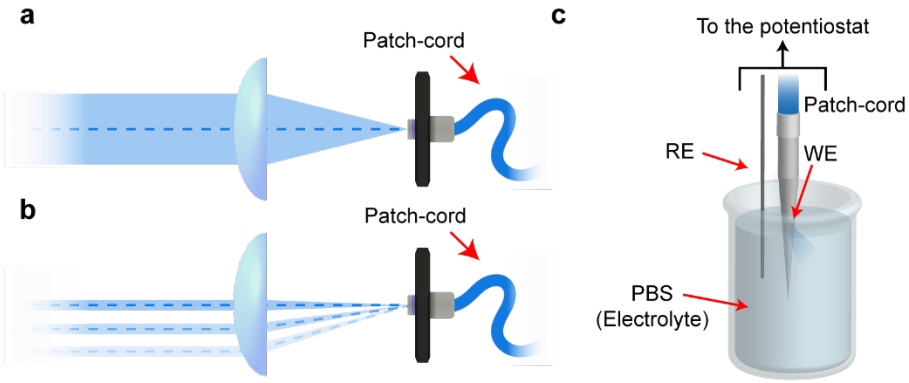

Supplementary Figure 5: In vitro configuration: Schematic representation of **(a)** the full NA and **(b)** angled light injection paths used to fit the conditions of Figure 5. **(c)** Schematic of the in vitro recording configuration.

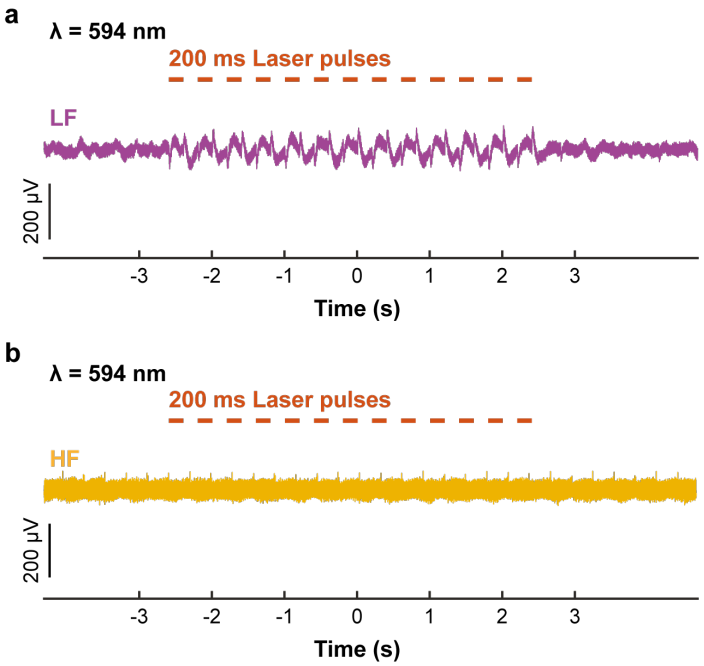

Supplementary Figure 6: Photoelectric artefacts characterization with light input wavelength of 594 nm. (a) LF filtered trace (1 - 100 Hz) recorded with a one-window one-electrode fibertrode (electrode diameter 15 µm, window size 20 × 20 μm^2) for a 594 nm light train (200 ms pulse duration), light input of 2 mW at the taper. **(b)** HF filtered trace (highpass filter, cutoff frequency 300 Hz) for the same device and light parameters used in **a**.

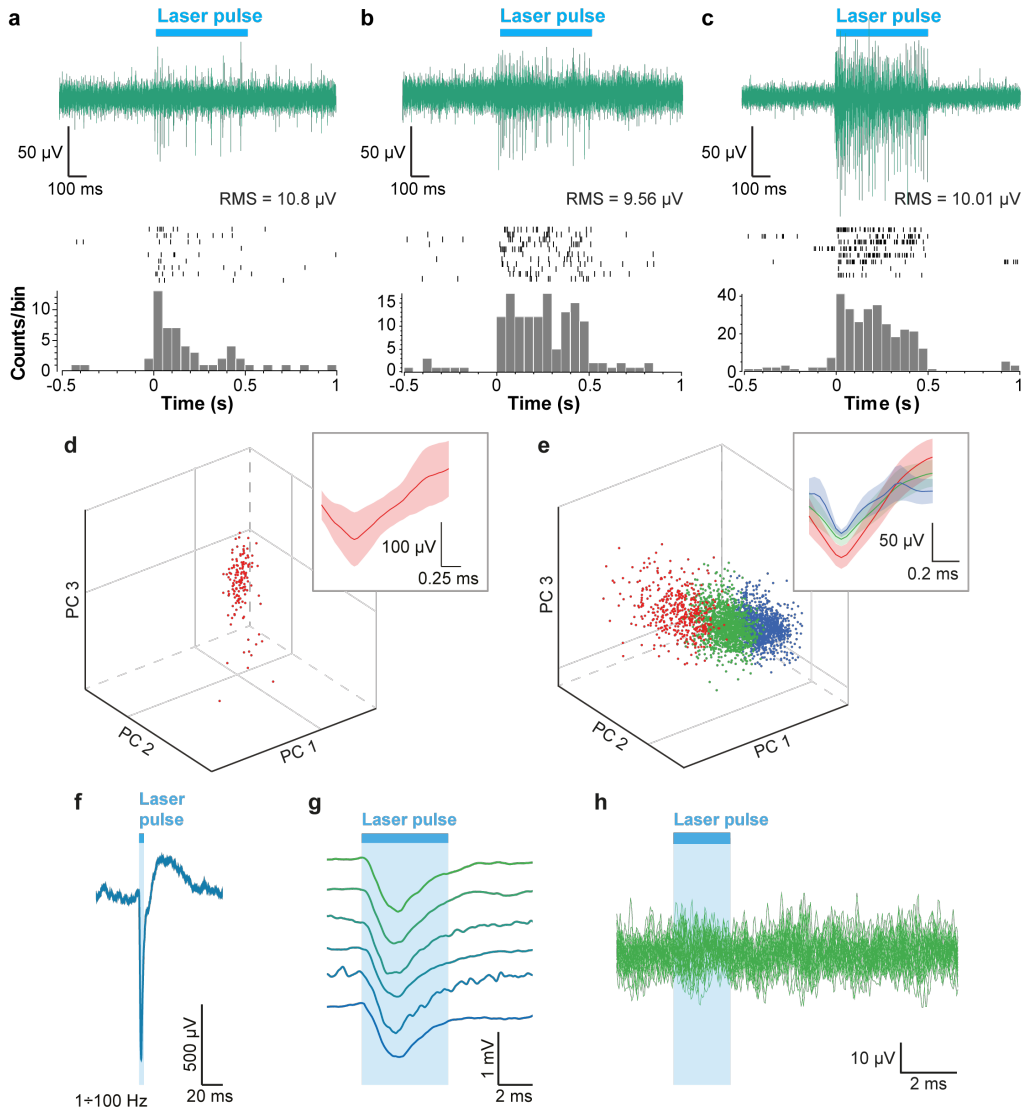

Supplementary Figure 7: In vivo Top - Representative traces and raster plots of action potentials recorded in striatum of Adora2A-Cre x ChR2f/f mouse with a fibertrode in response to continuous 500 ms optical pulse. Bottom – Average peristimulus histogram of the number of action potentials for **(a)** 7.5 µm electrode pad and 20 × 20 µm^2 window, **(b)** 7.5 µm electrode pad and 60 × 60 µm^2 window and **(c)** 30 µm electrode pad and 60 × 60 µm^2 window, respectively. Inter-trial interval was set to 30 s. **(d-e) Principal Component Analysis** of the first three principal components of the sorted units for **(d)** the slot with two electrodes probe and **(e)** the one window one electrode probe configurations, shown in **Figure 5**. In the inset, the sorted waveforms are shown, using the same data visualized in **Figure 5**, and following the same color scheme. Continuous line represents mean value and shaded area standard deviation of the sorted waveforms. Per-unit sort quality: L-Ratio$_a$ = 0.04 (green); L-Ratio$_b$ = 0.22 (red); L-Ratio$_c$ = 0.06 (blue); isolation distance isoD = 11.5. Cluster cutting ellipses are displayed at a confidence value of ~95%. **(f-h) LFP signals**. **(f)** LFP deflection recorded in response to 5 ms optical stimulation, average of 6 traces shown in g. **(g)** Individual traces of average LFP response depicted in f. **(h)** Overlapped 12 ms long traces in the LFP frequency range aligned at the onset of the laser (2 ms long pulses) in a wild-type mouse, measured with a one window-one electrode fibertrode.

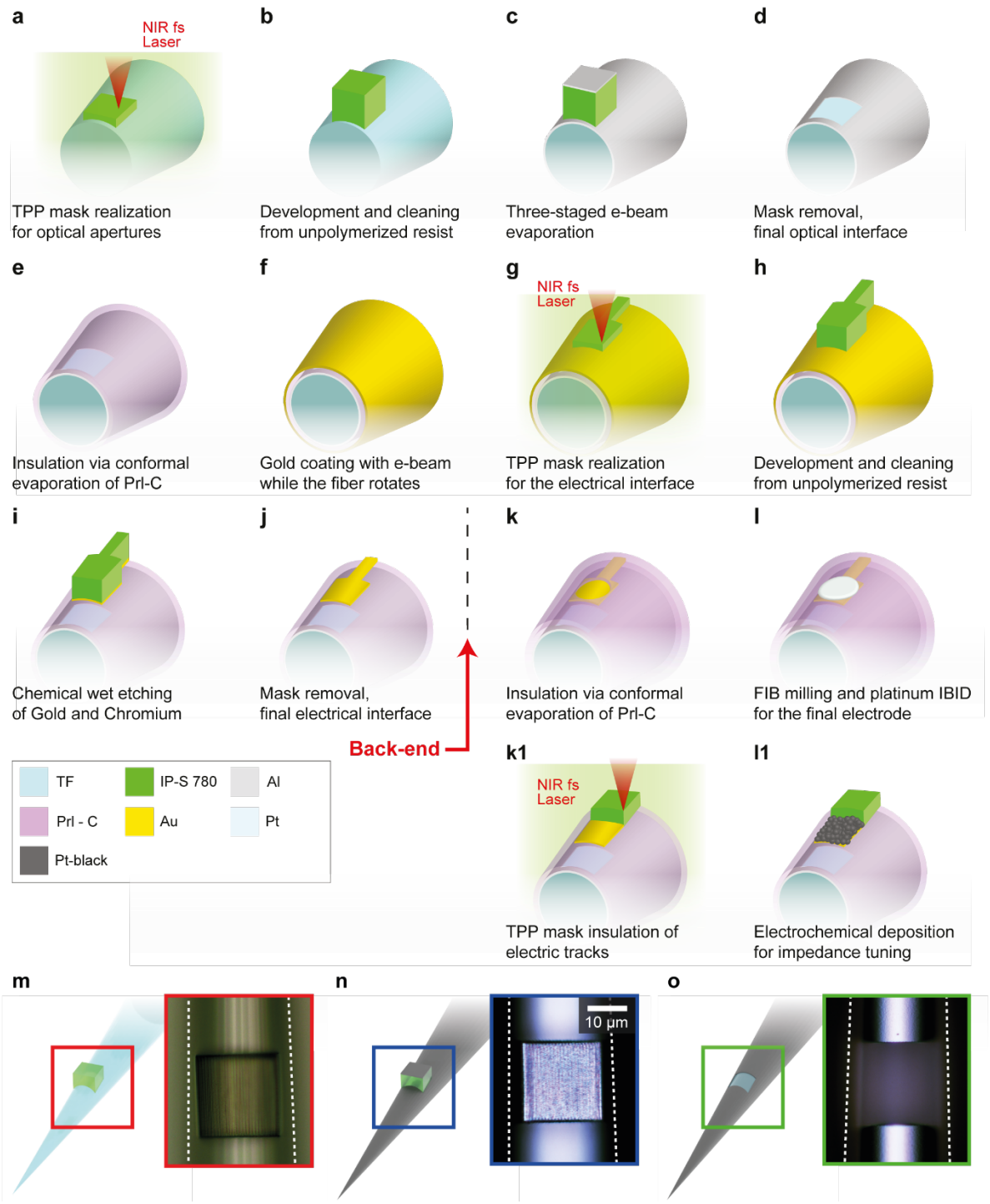

Supplementary Figure 8: (a-l) Two-photon polymerization process Schematics of the 2PP based process. **(m-o) Principal steps for the realization of optical apertures for µTFs via the 2PP based process. (m)** A 2PP 3D structure is realized on a bare TF. **(n)** The fiber and the structure are metal-coated through a three-staged thermal evaporation. **(o)** The 2PP structure is removed, leaving an uncovered surface on the TF edge, which shape corresponds to the projection on the TF surface of the 2PP volume. By means of illustration, next to each fabrication step sketch, optical microscope images of the fabrication of a 20 × 20 µm^2 at a fiber radius of R = 15 µm are reported.

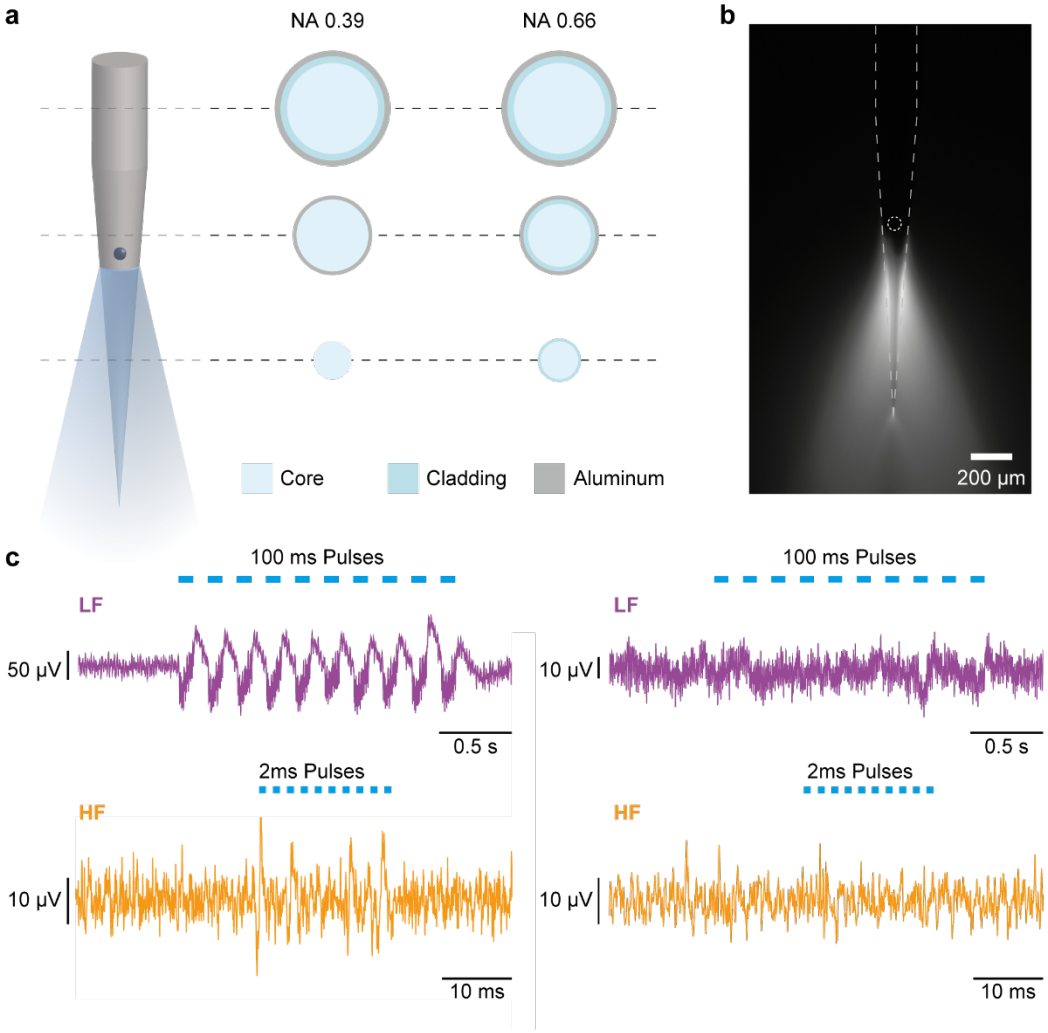

Supplementary Figure 9: Wide volume fibertrode. (a) Specific design for wide volume illumination can prevent light from impinging on the electrode. Tapering procedure leads to cladding removal in 0.39 NA optical fibers, while it is preserved in 0.66 NA fibers. **(b)** Light emission pattern in fluorescein. **(c)** In vitro characterization of the photoelectric artefacts referred to **(left)** 0.39 NA and **(right)** 0.66 NA optical fibers: artefacts in the low frequency channel are absent when the fiber cladding is intact (right, purple trace).

Figure	Setup	Bandwidth	SNR	σ_{noise}	N° of units	L-Ratios	Iso-distances
2 c,d	A-M Systems	300 Hz – 10 kHz	8.68	7.28 µV	2	(Unit A) 0.0004 (Unit B) 0.00007	27.99
2 e	T&D	250 Hz – 10 kHz	11.17	21.8 µV	3	(Unit A) 0.04 (Unit B) 0.06 (Unit C) 0.05	12.3
2 g,h	T&D	250 Hz – 10 kHz	Ch1 13.6	3.54 µV	2	(Unit A) 0.0004 (Unit B) 0.00007	39.4
			Ch2 8.77	6.56 µV	1	-	-
6 b,c	A-M Systems	300 Hz – 10 kHz	9.24	8.84 µV	-	-	-
6 e,f	T&D	250 Hz – 10 kHz	Ch1 6.79	8.8 µV	0	-	-
			Ch2 11.85	19.7 µV	1	-	-
6 h	T&D	250 Hz – 10 kHz	ChR2 8.37	13.2 µV	3	(Unit A) 0.04 (Unit B) 0.22 (Unit C) 0.06	11.5

Supplementary Table 1: Summary of the recording systems settings and obtained quality metrics in PCA analysis.